High Speed Multiple View Image Point Correspondences Using Rectification

D.D.A.P. Ariyawansa and T.A. Clarke

Optical Metrology Centre
Department of Electrical, Electronic and Information Engineering
City University, Northampton Square,
London EC1V 0HB, U.K.

Abstract

In high precision close-range applications, images of signalising targets on object(s) are acquired from multiple view points. Sub-pixel locations (image points) of target images are computed. In order to estimate 3-D locations, image point in each view that represent the same 3-D object point are identified. This identification process is referred to as establishment of image point correspondences and is the topic of this paper. The development of a multiple view image point correspondence algorithm based on rectification principles is discussed. The algorithm uses parallel epipolar lines for the establishment of image point correspondences hence, it is termed the Parallel Epipolar Line (PEL) algorithm. The PEL algorithm is suitable for applications where real-time multiple view image point correspondences are required.

Key words: epipolar, convergent, multiple views, image point, correspondences, rectification, real-time, 3-D measurement.

1. Introduction

Images acquired from different view points are considered as a set of stereo pair combinations and correspondences are established at the stereo pair level. Located image points of interest in a pair of convergent optical axis images are transformed into a pair of virtual images which lie on a single plane that is parallel to the base line of the convergent axis stereo pair. Virtual images have parallel local co-ordinate systems. This transformation is usually known as rectification and the resulting virtual images are termed rectified images. Correspondences are established in rectified image space with reduced searching resulting a faster correspondence solution. The PEL algorithm requires an initialisation stage during which a number of parameters are determined for each stereo pair combination. In terms of correspondence speed, PEL algorithm out performs the Epipolar line (EL) and 3-D Space Intersection (3DSI) correspondence algorithms when the number of points to be corresponded are greater than about 75 and 25 respectively. The lower speed performance for fewer than 75 and 25 points in each case is due to the overhead of parameter computation. The algorithm has a predictable speed performance as the time to solve correspondences increases approximately linearly for increasing numbers of image points.

2. Epipolar geometry and it's application to image point correspondences

Epipolar geometry is a fundamental projective relationship that exists between a pair of images. Considering a stereo pair, if the relative or absolute orientation of the images are known epipolar geometry can be used to define a search space. Figure 2.1 illustrates the formation of image points $p_{1i}(x_{1i},y_{1i})$ and $p_{2i}(x_{2i},y_{2i})$ of the 3-D world point $A_i(X_i,Y_i,Z_i)$ on a convergent axis image pair I_1 and I_2 where O_1 and O_2 are the optical centres. The line O_1O_2 is termed the base line. Points $e_1(x_{e1},y_{e1})$ and $e_2(x_{e2},y_{e2})$ are termed epipoles and are images of the optical centres O_2 and O_1 on images I_1 and I_2 respectively. Epipolar geometry states that five points A_i,O_1,O_2,p_{1i},and p_{2i} lie on a single plane which is termed the epipolar plane (Haralick and Shapiro, 1993). Image planes I_1 and I_2 intersect with the epipolar plane along lines l_{1i} and l_{2i} which are termed epipolar lines. Hence, for any image point that lies on the epipolar line l_{1i} of image I_1, the corresponding point in the image I_2 can be found by searching along conjugate epipolar line l_{2i}. This is termed the epipolar constraint. However, due to random and systematic errors in real imaging systems there is a deviation from this ideal imaging geometry. The corresponding points in image I_2 will not lie exactly on the epipolar line, hence a search needs to be performed within a band which symmetrically covers either side of the epipolar line. The appropriate width of the search band can be determined using the 2-D image residuals. Too large a band width may result in unwanted points coming into the band. Too small a band width may result in wanted points falling outside of the band.

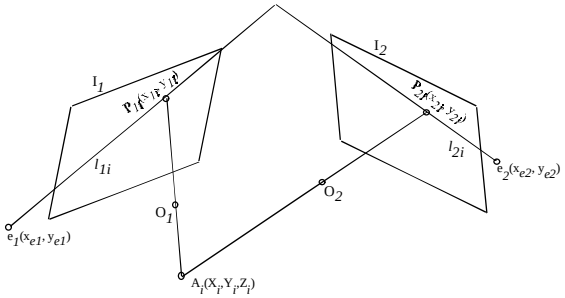

Figure 2.1 Epipolar geometry between convergent axis image pair

Considering point $p_{1i}(x_{1i},y_{1i})$ in image I_1, application of epipolar constraint limits the search space in image I_2 to within a band. Provided an appropriate search band width is used, the usual result is that a number of potentially corresponding or ambiguous points, in addition to the correct corresponding point, will exist within the search band depending on the image point density. Multiple images acquired from other view points can be used to solve these ambiguities.

3. Multiple view image point correspondence algorithms

There are a number of algorithms available for establishment of image point correspondences which use geometric and/or radiometric information (Chen and Clarke, 1994; Mass, 1992; Atkinson, 1996). In this section, implementation of the EL and the 3DSI algorithms are discussed which establish image point correspondences based on geometric information. Each algorithm has two stages. Initially, multiple images acquired from different view points are considered as a combination of stereo pairs. The epipolar constraint is applied to each stereo pair and potential correspondences are established. Secondly, the obtained information at stereo pair level is used to solve the ambiguities and distribute correspondences among all images.

3.1 Epipolar line (EL) algorithm

Figure 3.1 illustrates a set of images acquired from three view points. Images of a 3-D object point $A_i(X_i,Y_i,Z_i)$ in images I_1, I_2, I_3 are $p_{1i}(x_{1i},y_{1i})$, $p_{2i}(x_{2i},y_{2i})$, and $p_{3i}(x_{3i},y_{3i})$. Considering 3-D point $A_i(X_i,Y_i,Z_i)$ and image points p_{1i}, p_{2i}, and p_{3i}, epipolar geometry between image pairs I_1/I_2, I_2/I_3, and I_3/I_1 creates three epipolar planes whose intersections with image planes creates pairs of conjugate epipolar lines l_{12}/l_{21}, l_{23}/l_{32}, and l_{31}/l_{13} respectively.

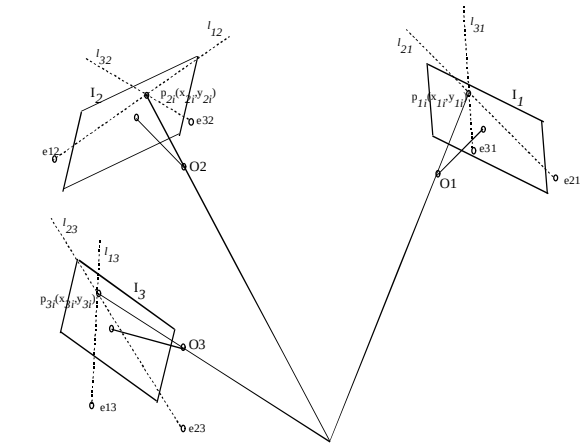

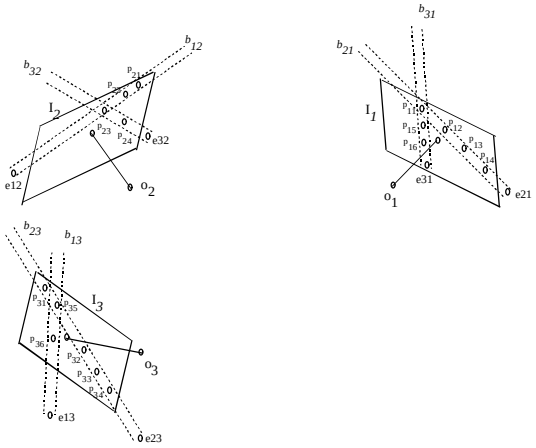

Figure 3.1 Epipolar geometry between three images

Figure 3.2 Application of epipolar constraint

Under ideal geometric conditions, pairs of epipolar lines (l_{21},l_{31} on image I_1; l_{12},l_{32} on image I_2; and l_{13}, l_{23} on image I_3) intersect on image points p_{1i}, p_{2i}, and p_{3i} forming a closed loop of image points. But in reality a parallel band covering either side of the ideal epipolar line is required. Figure 3.2 illustrates the application of the epipolar constraint to images acquired from three view points. The three image situation can be considered as three stereo pairs, I_1/I_2, I_2/I_3, and I_3/I_1. The epipolar constraint is applied to each pair separately and potentially corresponding points that lie within search bands are found. Assume that points p_{11}, p_{23}, and p_{35} in images I_1, I_2, and I_3 are corresponding. Consider point p_{11} in image I_1 and stereo pair I_1/I_2, it can be seen that points p_{21}, p_{22}, p_{23} fall within band b_{12} in image I_2 hence are potentially corresponding to point p_{11}. Now considering point p_{23} in image I_2 and stereo pair I_2/I_3, it can be seen that points p_{31}, p_{32}, p_{33}, p_{34}, and p_{35} fall within band b_{23} in image I_3 hence are potentially corresponding to point p_{23}. Finally considering point p_{35} in image I_3 and stereo pair I_3/I_1, it can be seen that points p_{11}, p_{15}, p_{16} fall within band b_{31} in image I_1 hence are potentially corresponding to point p_{35}. Thus obtained correspondence information can be represented in the form of a tree (Figure 3.3). Points that form a closed-loop in which a search path that begins and ends with the same point identity number can be taken as corresponding points. It can be seen from step-3 that one of the potentially corresponding candidates for p_{35} in image I_1 is the same point that was initially considered (p_{11}). Hence, points p_{11}, p_{23}, and p_{35} form a closed loop and are taken as corresponding. Potentially corresponding candidates for points p_{22} and p_{21} in image I_3 are not shown for simplicity.

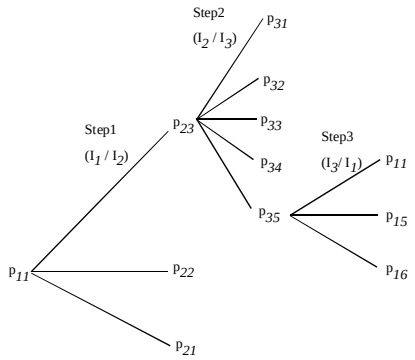

Figure 3.3 A tree of potentially corresponding image points

It is possible that there exist multiple paths that begin and end with the same identity number. Tests with simulated and real image data show that when the number of views is more than three, multiple paths are encountered more frequently due to the geometry between image and 3-D world points. These ambiguous situations can be solved by applying the epipolar constraint between different combinations of images. For instance, in the case of four convergent axis images I_1,I_2,I_3,and I_4 acquired from four view points, correspondences are first established using combinations I_1/I_2, I_2/I_3 I_3/I_4, and I_4/I_1. Any ambiguities that exist can be solved by considering stereo pair combinations I_1/I_3 and I_2/I_4. Unsolvable situations could occur when image points are very close such that the distance between points is less than the search band width. The discussion thus far applies to situations where each image views the same set of 3-D world points. Additional complications may occur if 3-D points are occluded or are out of the field of view of some images. In such situations it is possible that incorrect correspondences are established. When camera exteriors are accurate, 3-D intersection and subsequently computed 2-D image residuals can be used to detect most incorrect correspondences.

3.2 3-D space intersection (3DSI) algorithm

This algorithm applies the epipolar constraint in the 3-D object space rather than in the 2-D image space (Chen et al. 1994). It uses the fact that a pair of rays projected into 3-D space from corresponding image points should intersect at a single point on the epipolar plane which is the corresponding 3-D world point. In reality, due to errors of the imaging system these rays normally intersect with a small perpendicular distance D between them which is given by,

$$D = \begin{vmatrix} (X02 - X01) & (Y02 - Y01) & (Z02 - Z01) \\ p1 & q1 & r1 \\ p2 & q2 & r2 \end{vmatrix} \Bigg/ \sqrt{\begin{vmatrix} p1 & q1 \\ p2 & q2 \end{vmatrix}^2 + \begin{vmatrix} q1 & r1 \\ q2 & r2 \end{vmatrix}^2 + \begin{vmatrix} r1 & p1 \\ r2 & p2 \end{vmatrix}^2}$$

where, (X_{01},Y_{01},Z_{01}) and (X_{02},Y_{02},Z_{02}) are optical centres. $p = (m_{11}x + m_{21}y - m_{31}f)$, $q = (m_{12}x + m_{22}y - m_{32}f)$, and $r = (m_{13}x + m_{23}y - m_{33}f)$ where m_{11}, m_{12}, m_{13}, m_{21}, m_{22}, m_{23}, m_{31}, m_{32}, and m_{33} are rotational parameters and f is the focal length. Using the statistical knowledge of 3-D point location errors, a value for D (equivalent to search band width in the EL algorithm) can be determined to distinguish potentially corresponding points. In a multiple view situation, each stereo pair combination is considered separately, the constraint is applied, and potential candidates are identified. Using this information, ambiguities are removed and correspondences are distributed among all images as discussed for the EL algorithm. Therefore, apart from the way epipolar constraint is used at stereo pair level both algorithms have a similar implementation.

4. Multiple view image point correspondences using rectification - PEL algorithm

This algorithm has a similar implementation to the EL line algorithm. Correspondences are established between stereo pair combinations and are then distributed among all images. The advantage of this algorithm is the reduced searching that is required to find correspondences in stereo pairs. Assuming a stereo pair with n points in each image, previously discussed algorithms require searching which is proportional to n^2. Hence, time requirement increases non-linearly for increasing number of points. The PEL algorithm require searching which is approximately proportional to n. Hence, time requirement increases approximately linearly. Figure 4.1 illustrates a pair of convergent images I_1/I_2 and corresponding rectified images

I_{r1}/I_{r2}. The optical centres O_1 and O_2 are common to convergent and rectified images. Points p_{1i} and p_{2i} are the images of 3-D world point A_i on images I_1 and I_2. Due to the position and orientation, epipolar plane formed by points A_i,O_1,O_2,p_{1i}, and p_{2i} intersect rectified image planes along parallel and collinear epipolar lines l_{r1i} and l_{r2i}. Images of the same 3-D point A_i on images I_{r1} and I_{r2} (i.e. points p_{r1i} and p_{r2i}) lie on these epipolar lines. Hence, for a selected point in image I_{r1}, corresponding point can be found by searching along the conjugate epipolar line l_{r2i}. Correspondence process begins with the transformation of points from a pair of convergent images to a pair of rectified images. Image point location errors that exist in convergent images are automatically transferred into rectified images. Hence, a search is required to be performed along a band that covers either side of the epipolar line. The rest of this section describes each stage of the development of the algorithm and it's speed performances.

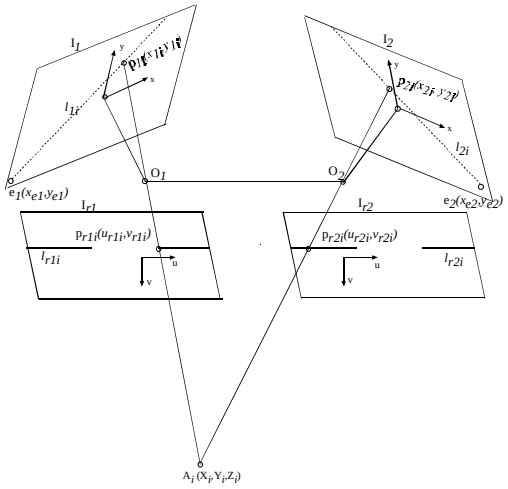

Figure 4.1 Convergent and corresponding rectified image pairs

4.1 Determination of unknown parameters of the algorithm

During the initialisation process of the algorithm, unknown parameters are determined. Considering a stereo pair, rectified image plane, rotational parameters of rectified images, and convergent to rectified image point transformation parameters (i.e. rectification parameters) need to be determined. Once rectification parameters are known, points in convergent images can be transformed into rectified images. The next step is the establishment of correspondences. As in convergent image space, a search band is required to constrain the search for corresponding points. Using a geometric relationship that exist between convergent and corresponding rectified image planes, search band parameters are also be determined during the initialisation.

4.1.1 Rectified image plane and rotational parameters

Rectified image plane:
This algorithm was developed with the rectified image plane positioned perpendicular to the reference plane formed by points O_1,O_2, and reference point R_r (Figure 4.2). The rectified image plane is parallel to the baseline O_1O_2. The perpendicular distance to this plane from baseline O_1O_2 is the focal length of the rectified images. The orientation of the reference plane is used to determine rotational parameters of the rectified images.

Figure 4.2 Reference plane $O_1O_2R_r$ **Figure 4.3 Co-ordinate systems on rectified images**

The principal rays pr_1 and pr_2 of images I_1 and I_2 intersect the XY-plane of the world co-ordinate system at points $R_1(X_1,Y_1,Z_1)$ and $R_2(X_2,Y_2,Z_2)$. Reference point $R_r(X_r,Y_r,Z_r)$ is the mid point of the line joining points R_1 and R_2. A unit vector *u* which is perpendicular to plane $O_1O_2R_r$ can be determined by taking vector product between vectors O_1R_r and O_2R_r as,

$$\bar{u} = \left(\frac{\overline{O_1R_r} \times \overline{O_2R_r}}{\left|\overline{O_1R_r}\right|\left|\overline{O_2R_r}\right| sin\left(O_1R_rO_2\right)} \right)$$

Angle $O_1R_rO_2$ is obtained by taking scalar product between vectors O_1R_r and O_2R_r as, $angle(O_1R_rO_2) = \cos^{-1}\left(\frac{\overline{O_1R_r}.\overline{O_2R_r}}{\left|\overline{O_1R_r}\right|\left|\overline{O_2R_r}\right|} \right)$.

Point R_p is on the base line O_1O_2. Co-ordinates of any point on line O_1O_2 can be written in parametric form as, $X = X0_1 + t\left(X0_1 - X0_2\right)$, $Y = Y0_1 + t\left(Y0_1 - Y0_2\right)$, and $Z = Z0_1 + t\left(Z0_1 - X0_2\right)$ where *t* is a variable. Vectors O_1O_2 and R_pR_r are perpendicular. Hence, the scalar product between vectors R_pR_r and O_1O_2, $\overline{R_pR_r}.\overline{O_1O_2} = 0$.

∴ *t* can be evaluated as, $t = \left(\frac{\left(\left(X_2 - X0_1\right)\left(X0_2 - X0_1\right) + \left(Y_2 - Y0_1\right)\left(Y0_2 - Y0_1\right) + \left(Z_2 - Z0_1\right)\left(Z0_2 - Z0_1\right)\right)}{\left(\left(X0_2 - X0_1\right)^2 + \left(Y0_2 - Y0_1\right)^2 + \left(Z0_2 - Z0_1\right)^2\right)} \right)$

Knowing *t*, the co-ordinates of point $P(X_p,Y_p,Z_p)$ can be calculated.

Rotational parameters:

With respect to plane $O_1O_2R_r$, the local co-ordinate systems of rectified images have directions as illustrated in Figure 4.3. In general, it can be stated as: **x-axis** is along the line created by intersection of rectified image plane and reference plane $O_1O_2R_r$; **y-axis** is perpendicular to plane $O_1O_2R_r$ and has the direction of unit vector *u*; **z-axis:** lies on the plane $O_1O_2R_r$ and has the direction of vector R_pR_r.

Once the orientation of co-ordinate systems on the rectified images are established, the world co-ordinate system XYZ can be rotationally transformed to obtain the same orientation as the rectified image co-ordinate system xyz (Figure 4.4). Three rotational parameters ω, ϕ, and κ are determined by sequential rotations around X,Y, and Z axis.

From triangle ABR_r, magnitudes of AB and Br_r can be obtained as $\left|AB\right| = \left(Y_p - Y_r\right)$ and $\left|BR_r\right| = \left(Z_p - Z_r\right)$. Hence, $\left|AR_r\right| = \sqrt{\left(Y_p - Y_r\right)\left(Y_p - Y_r\right) + \left(Z_p - Z_r\right)\left(Z_p - Z_r\right)}$.

From triangle AR_pR_r, magnitude of AR_p can be obtained as $\left|AR_p\right| = \left(X_p - X_r\right)$. Hence, ω and ϕ can be obtained as $w = angleAR_rB = tan^{-1}\left(\frac{AB}{BR_r}\right)$, and $f = angleAR_rRp = tan^{-1}\left(\frac{AR_p}{AR_r}\right)$.

Let a unit vector perpendicular to plane AR_pR_r be *v*. Taking vector product between vectors $\overline{R_pA}$ and $\overline{R_rA}$,

$\bar{v} = \frac{\overline{R_pA} \times \overline{R_rA}}{\left|R_pA\right|\left|R_rA\right| sin\left(angleR_pAR_r\right)}$ where angle $R_pAR_r = 90°$. Hence $\bar{v} = \frac{\overline{R_pA} \times \overline{R_rA}}{\left|R_pA\right|\left|R_rA\right|}$.

κ is the angle between unit vectors *v* and *u*. Each unit vector should be in a direction so that each makes an angle greater than 90° with vector $\overline{BR_r}$. If this angle is smaller than 90°, the direction of particular unit vector needs to be reversed by multiplying it with -1. Taking scalar product between unit vectors *u* and *v*,

$$k = \cos^{-1}\left(\frac{\bar{u}.\bar{v}}{\left|\bar{u}\right|\left|\bar{v}\right|} \right)$$

By considering the direction cosines of the unit vector *u* (i.e. orientation of plane $O_1O_2R_r$), the signs of ω, ϕ, and κ can be determined for any pair of rectified images.

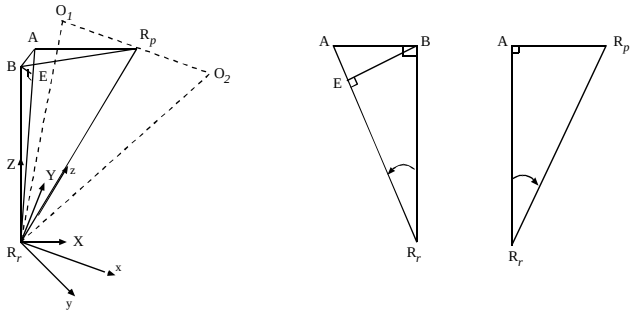

Figure 4.4 Transformation of XYZ to xyz

4.1.2 Rectification parameters

A point *(x,y)* in one image plane can be transformed into a point *(u,v)* in another non-parallel image plane using the following projective transformation equations (Wolf, 1983),

$$u = \frac{ax + by + c}{gx + hy + 1}, \quad v = \frac{dx + ey + f}{gx + hy + 1}$$ where *a,b,c,d,e,f,g,* and *h* are rectification parameters.

For a given stereo pair, two sets of rectification parameters are required. To determine each set of parameters, a minimum of four points are required that are well distributed in each rectified image space whose corresponding points in the corresponding convergent images are known. In this algorithm, four corner points of each convergent image are projected on to the XY-plane of the world co-ordinate system and are then reprojected back on to each corresponding rectified image plane to obtain four corresponding points. Substituting these co-ordinates into transformation equations results in eight equations that can be represented in matrix form as $AX = b$ where elements of matrices *A* and *b* of dimensions *(8x8)* and *(8x1)* are known. Hence, a set of unknowns can be determined as a *(8x1)* matrix, $X = A^{-1}b$. Then image points in convergent images can be transformed into rectified images.

4.2 Correspondences in rectified image space

Once image point co-ordinates are transformed into the rectified image space, the next task is the establishment of correspondences. As in the case of convergent images, a search band is required to constrain the search for corresponding points. Firstly, using a geometric relationship that exists between convergent and corresponding rectified images, the characteristics of search bands in rectified images are determined. Thus established relationship allows determination of parameters which are valid for any search band within the rectified image space. Hence, for any given epipolar line, it's search band can be established with minimal amount of computations. Preliminary correspondence speed performance tests were carried out and comparisons were made with other two algorithms discussed. Secondly, it is presented how the knowledge of search band parameters and boundaries of rectified images are used along with efficient sorting and searching methods to further speed up correspondence establishment.

4.2.1 Search band determination in rectified images

The area covered by a search band is defined by it's two border lines. If the parameters of border lines (i.e. slopes and intercepts) with respect to image co-ordinate systems are known, image points that lie within search band can be found. This section describes how search bands in rectified images are determined using the knowledge of corresponding search bands in convergent images. Search bands in convergent images can be transformed into rectified image space. Figure 4.5 shows a convergent image pair, a corresponding rectified image pair, and the search bands. In image I_2, a search band covering the epipolar line l_{2i} has border lines l_{1bi} and l_{2bi}. Corresponding epipolar line, and transformed border lines in rectified image I_{r2} are l_{r2i}, l_{r2bi}, and l_{r1bi}.

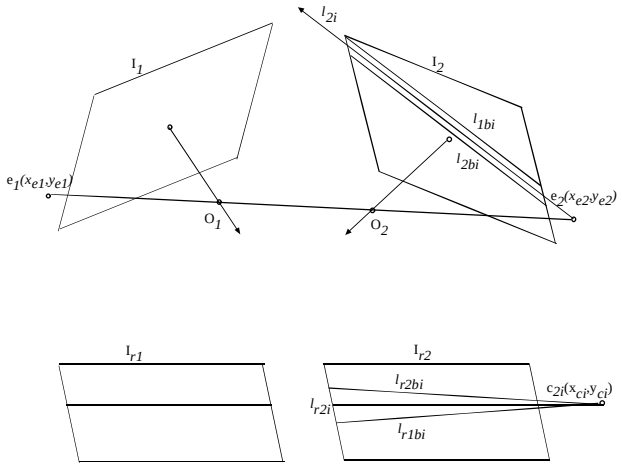

Figure 4.5 Transformation of search band from convergent to corresponding rectified image

The characteristics of the transformed search band border lines are dependant on the relative orientation between convergent image I_2 and corresponding rectified image I_{r2} which is dependant upon the relative orientation of the convergent image pair I_1 and I_2. Three stereo pairs whose approximate angular separation of optical axis 12°, 53°, and 80° were selected for simulation tests. Referring to Figure 4.5, a set of epipolar lines l_{2i} ($i = 1,....,n$) were created on image I_2 with regular angular spacing between them. Corresponding epipolar lines in rectified image I_{r2} are l_{r2i} ($i = 1,....,n$). The search band border lines in image I_2: l_{1bi}, l_{2bi} ($i = 1,....,n$) were transformed into rectified image I_{r2} resulting in corresponding border lines l_{r2bi}, l_{r1bi} ($i = 1,....,n$). A characteristic of any pair of border lines is that they intersect at a point $c_{2i}(x_{ci},y_{ci})$ which lies on the epipolar line l_{r2i} ($i = 1,....,n$). Each y-co-ordinate in rectified image space represent an epipolar line. The slopes and the crossing points of transformed border lines were noted for each stereo pair. Figure 4.6 illustrates slopes and x-co-ordinates of crossing points for varying y-co-ordinates for the stereo pair whose angular separation is 12°. The search band width in image I_2 was 0.016*mm* and focal lengths of rectified images were 32*mm* for this test.

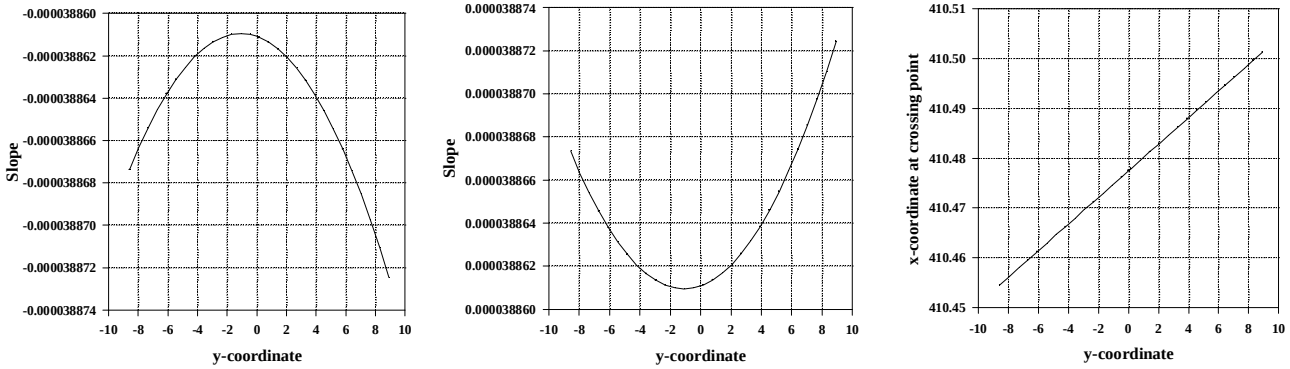

(a). border line l_{r1bi} **(b). border line l_{r2bi}** **(c). x-co-ordinate at crossing point of border lines l_{r1bi} and l_{r2bi}.**

Figure 4.6 Variation of search band border line slopes and their crossing points over whole rectified image

It can be seen (Figure 4.6 (a) and (b)) that the slopes have a symmetric variation with respect to y-co-ordinate. The variation of the slopes of either border line over the whole rectified image is about 1.1361×10^{-8} *mm*. As this is such a small variation, average values of slopes are considered as valid over the whole image. The other characteristic noted was that as the width of convergent image search band is increased, the slopes of transformed border lines on rectified images increases and vice versa. Hence, error caused due to the difference between average and actual values at any particular y-co-ordinate can be interpreted as a variation of the convergent image search band width. Maximum interpreted errors that could occur for different convergent image band widths (0.0016, 0.016, and 0.16*mm*) for this stereo pair are given in Table 4.1 and are negligible. When width is 0.0016*mm*, border line slopes are equal in magnitude. Hence, approximation errors and consequent interpreted search band variations are equal. As width increases, difference between slopes of a pair of border lines increases. Also the approximation errors and resulting interpreted variation of band width increases. The interpreted

error can be a reduction or increment of the search band width. But reduction is the largest in this case and is of importance as wanted points may fall out of the search band. For a given convergent axis stereo pair the characteristics of the rectified image search band depends only on the corresponding search band width of convergent image.

Search band width in convergent axis image (*mm*)	0.0016	0.016	0.16
Average of slopes of border lines (l_{r1bi}, l_{r2bi}) in rectified image	-3.886416×10^{-6}, 3.886416×10^{-6}	$-3.8864164 \times 10^{-5}$, 3.8864156×10^{-5}	$-3.88642004 \times 10^{-4}$, $3.88641196 \times 10^{-4}$
Maximum slope error due to approximation	8.29×10^{-10}, 8.29×10^{-10}	8.288×10^{-9}, 8.288×10^{-9}	8.288×10^{-8}, 8.288×10^{-8}
Reduction of convergent image bandwidth (*mm*)	$2 \times (3.4132 \times 10^{-7})$	$2 \times (3.4124 \times 10^{-6})$	$2 \times (3.4124 \times 10^{-5})$

Table 4.1 Maximum error in slopes and equivalent reduction of search band width in convergent image

The x-co-ordinates of the crossing point of search band border lines varies linearly as y-co-ordinate is varied. The variation of this quantity over the whole image is about 0.0478*mm*. For a given stereo pair, when rectified image focal length is increased the crossing point moves away from centre of image. The centre of the rectified image is referred as the point which is the base of the perpendicular from optical centre of image. Hence, the error that is caused by the difference between average and actual values can be interpreted as a variation of the rectified image focal length. The maximum error that could occur for this stereo pair is given in Table 4.2 and is negligible. For a given stereo pair crossing point is dependant only on the focal length of the rectified image. The interpreted error increases linearly as focal length increases.

Average of cross point x-co-ordinate (*mm*)	410.4779
Maximum error in x-co-ordinate (*mm*)	0.0234133
Change in rectified image focal length (*mm*)	0.0018

Table 4.2 Maximum error in x-co-ordinate and equivalent variation in rectified image focal length

Similar geometric analysis was carried out for the other two stereo pairs whose angular separations are 53° and 80°. It was noted that as angular separation increases, the slopes of rectified image search band border lines increases. For stereo pair with separation of 53°, the maximum interpreted convergent image search band width reduction due to approximations are $2x1.9241x10^{-5}$, $2x1.9241x10^{-4}$, and $2x1.9241x10^{-3}$*mm* for convergent image band widths 0.0016, 0.016, and 0.16*mm* respectively. The same quantities for stereo pair with separation of 80° are $2x3.3402x10^{-5}$, $2x3.3402x10^{-4}$, and $2x3.3402x10^{-3}$ *mm*. It can be seen that error increases as angular separation increases. However, error is only a smaller percentage of the size of the band, hence can be neglected. The size of this variation may be important when convergent image search band width is smaller. In the case of crossing point x-co-ordinate, interpreted error in rectified image focal length for the former was 0.007669*mm* and that for the later was 0.009809*mm*.

It can be concluded that as the angular separation increases, the angle between convergent and rectified image planes increases. There exist a strong geometric relationship between convergent and corresponding rectified image band characteristics regardless of the imaging sensor. Convergent image search band width depends on the resolution of the sensor and hence 2-D image residuals. The higher the resolution, the lower the 2-D image residuals and hence lower the band width. Pulnix TM-6CN CCD cameras which have been used for experiments have pixels of dimensions 8.4 x 8.2*mm*. Hence, a range of convergent image search band widths of 0.0016, 0.016, and 0.16*mm* were used for the purpose of this analysis. This foregoing analysis can be utilised to establish search band parameters in rectified image space. For any given epipolar line in rectified image, the search band border line slopes and x-co-ordinates of their crossing points are known once the initialisation process is complete. Hence points that lie within this search area can be found with less computations.

4.2.2 Preliminary speed performance tests

Tests were carried out with the PEL algorithm at this preliminary stage of development to assess it's performance. A Pentium processor based PC operating at 200MHz was used and the correspondence speed performances of PEL algorithm was compared with EL and 3DSI algorithms. For a varying number of densely distributed image points *n* (*n = 10 - 400*) in each image, the time taken by each algorithm to establish correspondences in a stereo pair was noted (Figure 4.7 (a)). No

occlusions were present as images were of a simulated co-planar target field. It can be seen that the 3DSI algorithm has poor speed performance compared to others. This is due to the costly minimum distance computations that are required to be performed n^2 times assuming n points in each image. The EL algorithm has better speed performance than the 3DSI algorithm due to less amount of computations required to be performed n^2 times. The PEL algorithm at this stage has better speed performance than the EL and the 3DSI algorithms when the number of image points n is greater than about 130 and 30 respectively (Figure 4.7 (b) and (c)). The PEL algorithm requires an n^2 search, but reduced computations due to the availability of pre-computed search band border line parameters, application of epipolar constraint involves less computations hence, it has better speed performances. For fewer than 130 and 30 points in each case, PEL algorithm has lower performance due to the overhead of parameter computation in the initialisation stage which takes 1mS for a stereo pair.

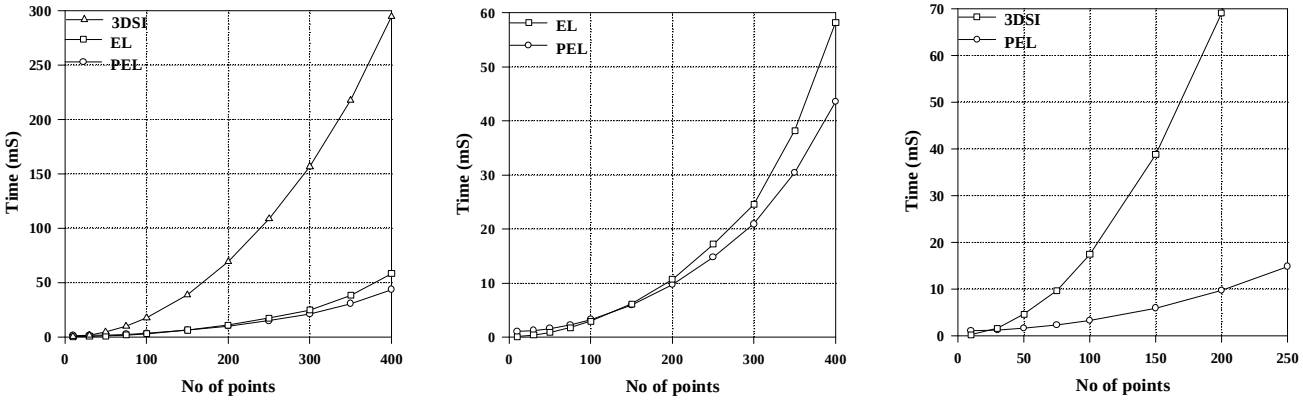

Figure 4.7 Speed performance of algorithms at stereo pair level

4.2.3 Rectified image point correspondences with improved speed performance

With the aforementioned knowledge of the characteristics of the search band border lines over the whole rectified image, the PEL algorithm can be made more efficient by avoiding the n^2 search. Increased efficiency is achieved by replacing the sloped border lines with those that are parallel to the epipolar line in the rectified image space. Figure 4.8 illustrates a pair of rectified images I_{r1}, I_{r2} and a pair of corresponding points p_{r1i} and p_{r2i}. Lines l_{r1i} and l_{r2i} are conjugate epipolar lines. l_{r1bi} *and* l_{r2bi} are search band border lines which are parallel to epipolar line l_{r2i}. d_1 and d_2 are perpendicular distances to the border lines from the epipolar line. Provided rectified image co-ordinates of both images are sorted in ascending order of y-co-ordinate, an efficient search can be performed to find corresponding points.

The algorithm uses knowledge about the co-ordinates of the transformed four corners of the convergent image on rectified image plane to determine distances d_1 and d_2. It was established that average values of the varying search band border line slopes and x-co-ordinates of their intersecting points are as valid over whole rectified image. Figure 4.9 illustrates an example of transformed four corner points cp_{r1i} and cp_{r2i} ($i=1,..,4$) on the rectified images I_{r1} and I_{r2}. The dotted lines at $x = x_{cr2}$ represent average values of the x-co-ordinates at the border line crossing points. Consider any point in image I_{r2} within the transformed area covered by four corners. The further away this point is from the $x = x_{cr2}$, the larger the vertical y-distance from it to either sloped border line. In the case of the transformed four corners, the vertical y-distances are maximum at corner point cp_{r21} which is the furthest away from line $x = x_{cr2}$. Points closer to $x = x_{cr2}$, produce smaller vertical y-distances. Hence distances d_1 and d_2 due to the corner point cp_{r21} are taken as valid over the whole rectified image. AC, BC are sloped border lines and AD, BE are corresponding parallel border lines.

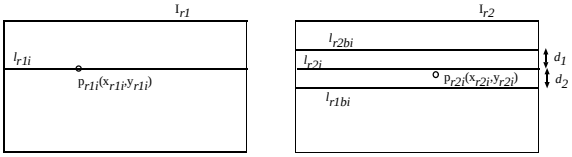

Figure 4.8 Parallel search band border lines in border rectified images

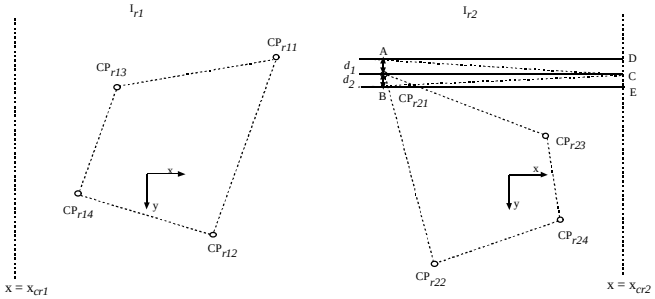

Figure 4.9 Transformed four corners and parallel lined search band in rectified image

A possible concern is that area covered by the parallel border lined search band is larger than that covered by sloped border lined search band. The result could be that unwanted image points may also fall within the band due to the larger area. Also the use of a single pair of distances as valid over whole image adds extra area to the search band. Table 4.3 illustrates the transformed furthest and nearest corner point co-ordinates to $x = x_{cr2}$, average values of border line slopes and x-co-ordinate at crossing points, and pairs of vertical y-distances to parallel border lines at the furthest and the nearest corner points for the same three stereo pairs considered previously. The convergent image search band width was 0.0016*mm*. Vertical distances due to furthest and nearest corner points produces maximum differences between them but are negligibly small.

Angular separation	Furthest and nearest transformed corners in	Averages of border line (l_{r1bi}, l_{r2bi}) slopes	Average of border line cross point x-co-ordinate (*mm*)	Vertical distances to border lines at furthest & nearest corner points	Difference between vertical distances (*mm*)
12°	(-12.1394, -7.4907), (6.7206, 7.1702)	-3.886416×10^{-6}, 3.886416×10^{-6}	410.4779	(0.001643, 0.001643), (0.001569, 0.001569)	0.000074 0.000074
53°	(-34.8585, -2.3610), (-3.9634, 1.4367)	$-2.2782120 \times 10^{-4}$ 2.2782133×10^{-4}	62.9484	(0.002232, 0.002232), (0.001521, 0.001521)	0.000711 0.000711
80°	(45.2081, 13.8779), (15.0632, -9.6412)	-3.218785×10^{-4} 3.218787×10^{-4}	-38.7281	(0.002708, 0.002708), (0.001729, 0.001729)	0.000979 0.000979

Table 4.3 Parameters of parallel search band border lines

Having determined separations d_1 and d_2, correspondences can be established by efficient searching through sorted image co-ordinates. Assuming *n* transformed points in each image, application of epipolar constraint only involves comparison of y-co-ordinates to check if a point falls within the band. Due to the reduced computations and searching, the PEL algorithm is more efficient. Previous speed performance tests were repeated. The time taken by a stereo pair for a varying number of points was noted (Figure 4.10(a)). The PEL algorithm now out performs EL and 3DSI algorithms when number of points are greater than about 75 and 25 respectively ((b) and (c)). The algorithm now takes 10*mS* as opposed to 43*mS* for correspondence of 400 points. The time taken now varies approximately linearly with increasing number of image points.

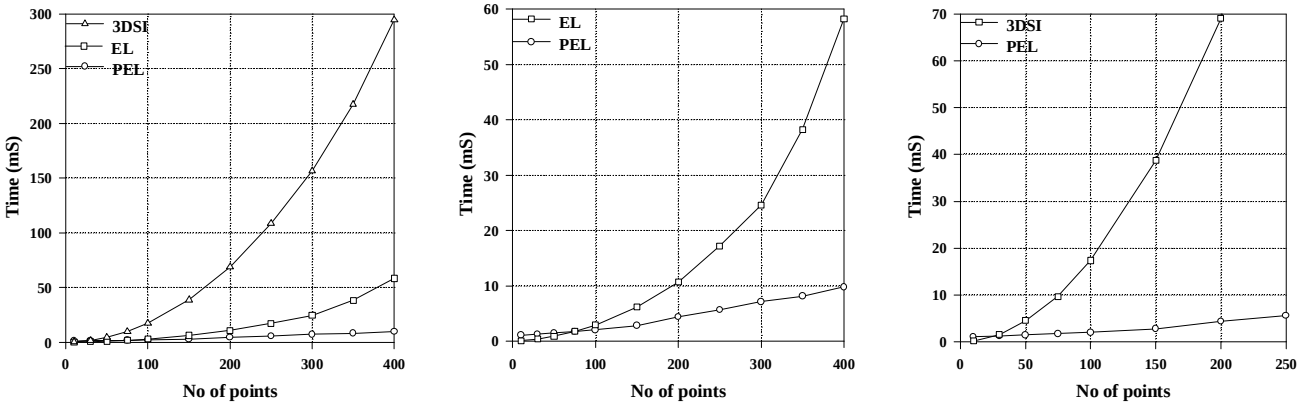

Figure 4.10 Speed performance of algorithms at stereo pair level with performance improved PEL algorithm

4.3 Speed performance of PEL algorithm in multiple view image point correspondences

As discussed previously, images acquired from multiple view points were considered as a combination of stereo pairs. Correspondences were established at stereo pair level and the geometric relationship discussed for the EL algorithm (3.1) was used for the distribution of correspondences. Timing tests were carried out with the same set of simulated co-planar 3-D points. For a varying number of image points, the time taken by each algorithm was noted (Figure 4.11(a)). The PEL algorithm is faster than each algorithm when the number of points is more than about 75 and 25 respectively. The time consumption varies linearly with increasing number of points. For 400 points, the PEL algorithm takes 60*mS* where as EL and 3DSI algorithms takes 350*mS* and 1.78*S* respectively. Hence, the PEL algorithm has the best correspondence speed performance. The predictable time consumption is also a favourable feature of the algorithm.

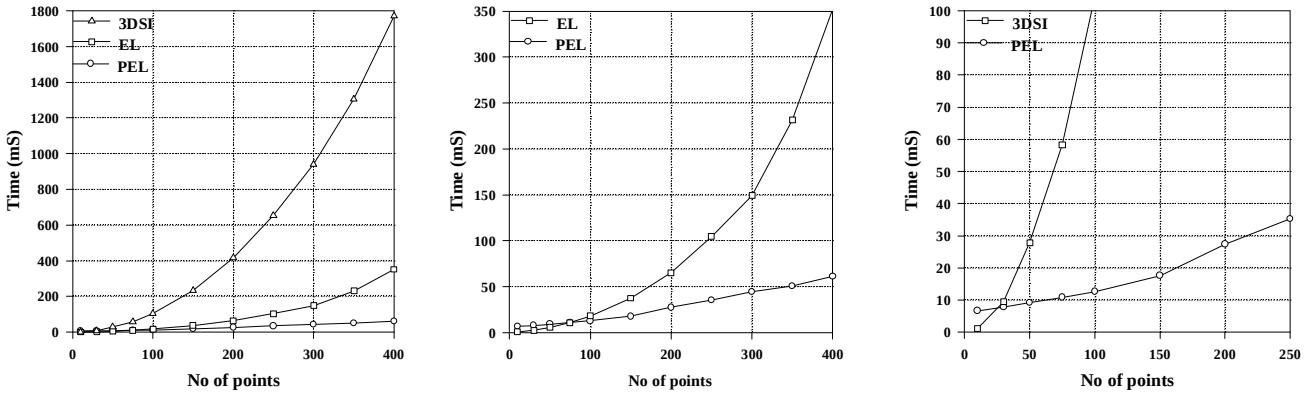

Figure 4.11 Speed performance of algorithms with four views

5. Experiments with real image data

Images of a densely distributed approximately planar retro-reflective target field were acquired from four different view points using Pulnix TM-6CN CCD cameras. Accurate camera exterior and internal parameters were available. The target images were identified, and their sub-pixel locations were computed. Resulting images point co-ordinates were corrected for lens distortions. Figure 5.1 illustrates sub-pixel locations of points in four images. From the 3-D adjustment process, standard deviations of image point location residuals and 3-D location errors were available. Using this information, an appropriate convergent image search band width was calculated.

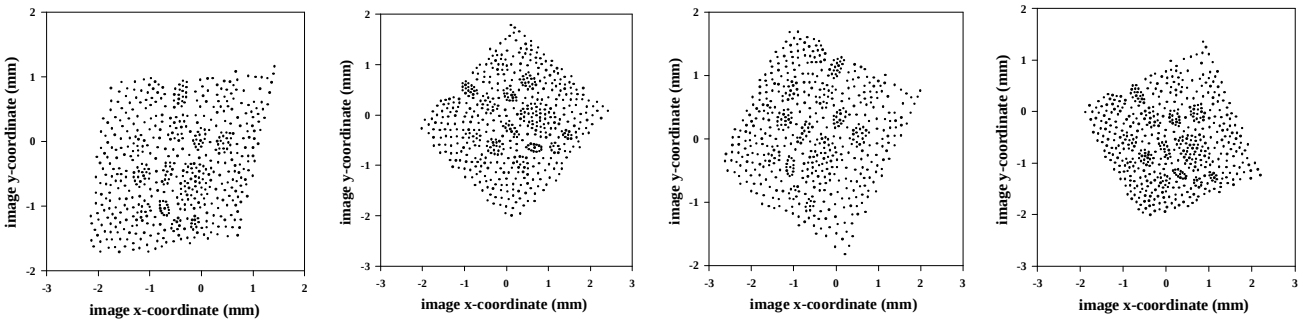

Figure 5.1 Located image points of a densely distributed target field on four views

Image point correspondences were established between all images using the PEL algorithm which required 87*mS*. The 3-D reconstruction of the coplanar target field illustrated in Figure 5.2. The correctness of point correspondences were checked using 3-D intersection and 2-D image point residuals.

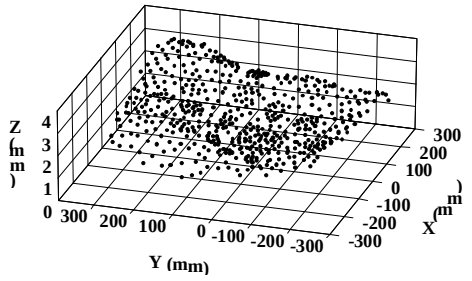

Figure 5.2 3-D reconstruction of the target field

6. Conclusions

In this paper, the theoretical development of a fast image point correspondence algorithm has been described. The practical use of the algorithm was illustrated using experiments with real image data. Complex situations due to occlusions etc. were not considered in these experiments. With a further step of development PEL algorithm will be able to cope with such situations. Speed performance comparisons were made with 3DSI and EL algorithms. The 3DSI algorithm has poor speed performance relative to other two algorithms due to n^2 searching which involves computational intensive minimum distance computations. The EL algorithm also requires n^2 searching but involves fewer computations in applying the epipolar constraint. Hence, it is more efficient compared to the 3DSI algorithm. Prior to the introduction of parallel search band border lines in rectified image space, the PEL algorithm also required n^2 searching. However, due to the availability of pre-computed sloped search band border line parameters, the epipolar constraint can be applied with fewer computations compared with the EL algorithm. Due to the time required for initialisation process, the PEL algorithm is efficient when number of image points is greater than 130. With the introduction of parallel search band border lines in rectified image space, searching becomes approximately proportional to *n*. Hence, the PEL algorithm has approximately linear time consumption as the number of image points increases.

7. Acknowledgements

Mr. D.D.A.P. Ariyawansa would like to acknowledge the support of The Worshipful Company of Scientific Instrument Makers in providing a PhD study bursary.

8. References

Ariyawansa, D.D.A.P. and Clarke, T.A. 1997. High speed correspondences for object recognition and tracking. SPIE Vol. 3174. Videometrics V, San Diego, U.S.A. pp. 70-79.

Atkinson, K.B. 1996. Close-range photogrammetry and machine vision. Published by Whittles Publishing, U.K. pp. 217-255.

Chen, J. Clarke, T.A. Cooper, M.A.R. Grattan, K.T.V.G. 1994. An optimised target matching based on a 3-D space intersection and a constrained search for multiple camera views. Videometrics III. SPIE Vol. 2350. Boston. pp. 324 - 335.

Haralick, R.M, and Shapiro, L.G. 1993. Computer and Robot Vision Volume II. Published by Addison-Wesley Publishing Company Inc. USA. pp. 289-366.

Mass, H. -G. 1992. Complexity analysis for the establishment of image correspondences of dense spatial target fields. Proc. ISPRS, XVIIth congress, Washington D.C., U.S.A. pp. 102-107.

Sommerville, D.M.Y. 1934. Analytical geometry of three dimensions. Published by Cambridge University , U.K. pp. 1-73.

Wolf, P.R. 1983. Elements of photogrammetry. 2nd edition .Published by McGraw-Hill. pp 559-614.

PAPER REFERENCE

Ariyawansa, D.D.A.P. and Clarke, T.A. 1999. High Speed Multiple View Image Point Correspondences Using Rectification, Videometrics VI, San Jose.